IEEE Access
Multidisciplinary ⋮ Rapid Review ⋮ Open Access Journal

Received 7 August 2024, accepted 18 August 2024, date of publication 21 August 2024, date of current version 6 September 2024.

Digital Object Identifier 10.1109/ACCESS.2024.3447095

RESEARCH ARTICLE

Prediction of Positive Lightning Impulse Breakdown Voltage Under Sphere-to-Barrier-to-Plane Air Gaps Using Machine Learning

JIN-TAE KIM[1] AND YUN-SU KIM[2], (Senior Member, IEEE)
[1]Korea Electric Power Research Institute (KEPRI), Daejeon 34056, South Korea
[2]Gwangju Institute of Science Technology (GIST), Gwangju 61005, South Korea

Corresponding author: Yun-Su Kim (yunsukim@gist.ac.kr)

This work was supported by the Gwangju Institute of Science Technology (GIST) Research Project grant funded by the GIST.

ABSTRACT Barrier, solid insulator, is inserted between conductors to make compact power equipment. Prediction of the dielectric strength is significant owing to nonlinear effect of barrier. In this paper, positive lightning impulse breakdown voltages are predicted under sphere-to-barrier-to-plane air gaps using machine learning algorithms including a support vector regression (SVR), Bayesian regression (BR), and a multilayer perceptron (MLP), which are rarely used to derive breakdown voltages. Previous studies have generally considered background electric fields in field arrangements that lacked barriers. In contrast, electrostatic features are suggested based on the electro-geometric equivalency of each electrode, electric field distributions between sphere and barrier or between barrier and plane, and a condition for stable penetration of discharge channels, influencing background fields and discharge propagation characteristics in air gaps. SVR yielded more precise Breakdown voltages than BR or MLP. Predictions from algorithms were in good agreement with experimental results, regardless of geometrical parameters such as spherical radius, gap distance and barrier width. In particular, the SVR-predicted voltages were even more accurate than the calculated voltages from streamer propagation method in strongly inhomogeneous field with barrier. Our proposed method derives breakdown voltages without the need to consider geometrical parameters affecting streamer propagation.

INDEX TERMS Bayesian regression (BR), barrier, lightning impulse breakdown voltage, multilayer perceptron (MLP), support vector regression (SVR), sphere-to-barrier-to-plane.

I. INTRODUCTION

Power equipment is becoming increasingly compact because it must be installed in confined spaces such as urban substation or the nacelle of wind turbines. As the spatial distance between current-carrying conductors decreases, the risk of electrical breakdown (BD) in energy storage systems or gas insulated medium-voltage switchgears increases. Therefore, the design of the dielectric strength is very important to withstand arbitrary disruptive voltages under operation. The dielectric strengths of power apparatuses must withstand voltages higher than the reference test voltages of International Electronical Committee (IEC) [1]. Thus, the prediction of breakdown voltages is essential.

Many studies have evaluated breakdown voltages based on various gases present and the geometric shapes of electrodes. Particle-in-cell and fluid models predict minimum ignition voltages over the very short gas gaps of extinguishing regions of circuit breakers and model electrical breakdown of air at *pd* values higher than Paschen minimum, which is based on the Paschen curves [2], [3]; the Paschen curve is one of traditional theoretical approaches to predict breakdown voltages,

The associate editor coordinating the review of this manuscript and approving it for publication was Wenbing Zhao.

based on the product of gap distance(d) and pressure(p), to control the number of generated electrons by nonlinear collision ionization which results in breakdown. This law can be only applied to quasi-uniform electric field distribution such as sphere-to-sphere air gaps. One traditional theoretical criterion when evaluating gas breakdown in non-uniform electric fields is streamer inception [4], [5], [6]; it is used when evaluating impulse and AC power frequency breakdown voltages of gases such as dry air, SF_6, CO_2, and mixtures thereof in non-uniform fields [7], [8], [9]; the ionization coefficients are directly considered to reflect the nonlinearity of the electron generation by collision. For such criteria to be applied successfully, both ionization coefficients and critical avalanche sizes are required. Ionization coefficients are affected by moisture; the critical avalanche sizes differ among gases [10]. As such data are rarely reported, efforts have been made to replace ionization coefficients by other parameters derived from Paschen curve or to calculate the critical avalanche size in air within pd of 100 bar·cm [11], [12]. Nevertheless, the streamer inception criterion is difficult to apply. A different criterion, streamer propagation, is mainly used when field distributions are strongly inhomogeneous fields such as needle-to-plane field arrangement or when the radius is much smaller than the air gap distance [13]; in the streamer propagation method, the potential of streamer head is required for nonlinear electron generation (by collisions) needed to generate the breakdown. The internal field strength behind the head of a streamer (E_{st}) is the average electric field (∼0.5 kV/mm) associated with at least a 90 % probability of complete breakdown and is influenced by voltage shape, humidity, and polarity [14], [15]. In these traditional methods, the product of pd, ionization coefficient and the potential of the streamer head are difficult to obtain within the practical ranges needed for applications. Also, a needle-to-barrier-to-plane electrode exhibits an electro-geometric equivalency [16], but the slopes of the equivalency differ by geometric shapes. Therefore, machine learning is required to predict breakdown voltages, because machine learning can individually consider geometrical design parameters and physical parameters affecting both the nonlinear electron generation and the discharge propagation, and analyze the effect of each parameter on complex breakdown process, based on calculated values of various electrical properties corresponding to geometrical shapes.

Neural networks have been used to evaluate breakdown voltages of transformer oils or partial discharges in power equipment [17], [18], [19]. A support vector machine (SVM) is employed to predict lightning impulse or AC power frequency breakdown voltages of air gaps between various geometric shapes, including parallel planes, rod-to-plane, and sphere-to-sphere geometries. Many electrostatic field features have served as inputs to SVM [20], [21], [22], but only some of these are used. Therefore, optimization methods are employed to reduce model complexity. Generic algorithms (GA) are effective in this regard [23]. Principle component analysis (PCA) is useful when choosing features that accurately reflect the electrical characteristics of electrodes, but not when such features do not reflect the electrical characteristics [24], [25]. Previous studies have found that background electric fields may not be adequately informative, depending on physical situations. Also, deep learning has been employed to evaluate motor partial discharge inception voltages (PDIVs) and to calculate the breakdown voltages of ball-to-ball electrodes in ultra-high-voltage apparatuses [26], [27]. However, this method can only evaluate problems which can be solved by the known features affecting phenomena of interest. Therefore, feature design is very important.

Features were selected based on background electric fields and discharge propagation characteristics of electrodes of certain geometric shapes. Background electric fields are determined by these shapes, and ionization is influenced by background electric fields. Moreover, streamers are followed by discharge channels. The conductivity of the streamer is lower than that of the discharge channel. The streamer propagation can be a precursor to the channel propagation. Therefore, streamer propagation capabilities have been investigated using electrostatic field parameters to indirectly analyze propagation characteristics of discharge channels associated with geometrical shapes. Machine learning algorithms that can evaluate breakdown voltages include a support vector regression (SVR), a Bayesian regression (BR), and a multilayer perceptron (MLP); all are used to train models. Two of these algorithms feature only one hidden layer but exhibit the high computational efficiency and the fast-processing time [28]. A multilayer perceptron (MLP) may have several hidden layers and can thus solve complex problems.

In this paper, sphere-to-barrier-to-plane electrodes were utilized as test electrodes to evaluate the dielectric strength of current-carrying conductors in the compact power equipment. Breakdown voltages of these electrodes are seldom analytically predicted via machine learning, so the positive lightning impulse breakdown voltages were predicted. The prediction accuracies of SVR, BR, and MLP were compared. Predicted voltages were compared based on the voltages derived using both the streamer propagation-based method and experimentally.

II. ELECTRIC FIELD SIMULATION UNDER ELECTRODES

Discharge ignites at the active (high voltage) sphere electrode under the sphere-to-barrier-to-plane air gap, because the discharge inception is closely associated with the maximum electric field. The maximum electric field is mainly determined by the radius and the gap distance under such given test electrodes. Furthermore, surface charges on the barrier surface form the electric potential and electrically shield the external potential of the active sphere electrode [29], [30]. Surface charges are influenced by the barrier position and width [29]. Therefore, these factors were experimentally and analytically considered.

A two-dimensional model of the sphere-to-barrier-to-plane system was built using a finite element method (FEM). A voltage of 1 kV was applied to the high voltage spherical electrode (copper) and the grounded potential was connected to the plane electrode (stainless steel). A zero charge density was initially applied to the surface of barrier (sheet molding compound; SMC) of dielectric constant 3.7. Figure 1. (b) presents a cloud chart of the electric field distribution. The strongest electric field is that around the spherical electrode. The breakdown (discharge) path is not shortest inter- electrode path that is used to calculate capacitive energies of the electrodes. Surface charges accumulate on the surface of barriers [30]. One method of calculation assumes that the surfaces are charged to saturation; thus, the normal field component vanishes at surfaces that face the air when calculating surface charges [31]. Then, surface charges can be calculated using equation (1):

$$\sigma_{sat,j} = \epsilon_{ins} E_{n,ins,j}, \tag{1}$$

where $\sigma_{sat,j}$ is the saturation charge that accumulates on the j-th element of a surface; ϵ_{ins} is the dielectric constant of the barrier; and $E_{n,ins,j}$ is the j-th normal electric field of air.

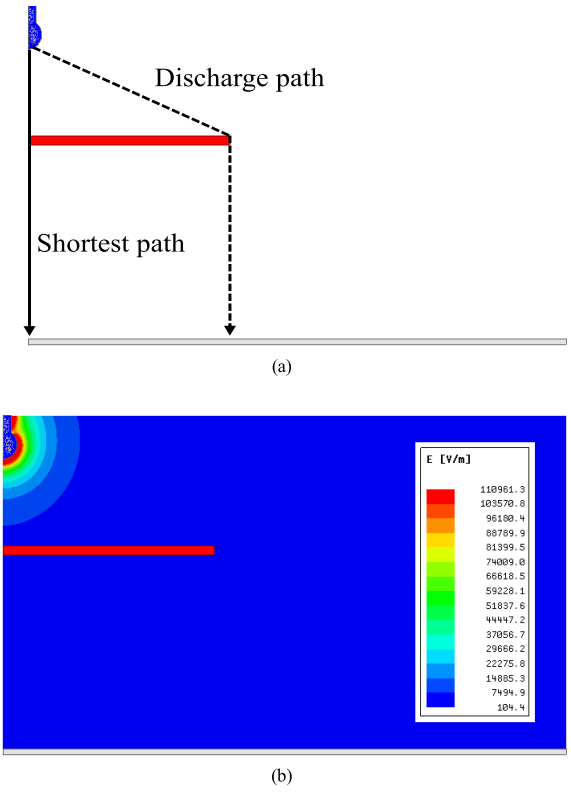

FIGURE 1. Electric field distributions by electrode shape: a) Sphere-to-barrier-to-plane electrode configuration, b) Electric field distribution. (r: 5 mm, gap distance: 100 mm, barrier width: 150 mm; voltage of 1 kV applied to sphere.).

III. BREAKDOWN EXPERIMENTS AND RESULTS FOR DATASETS

Figure 2 presents the experimental setup, which features an impulse generator, a measuring system, and test electrodes.

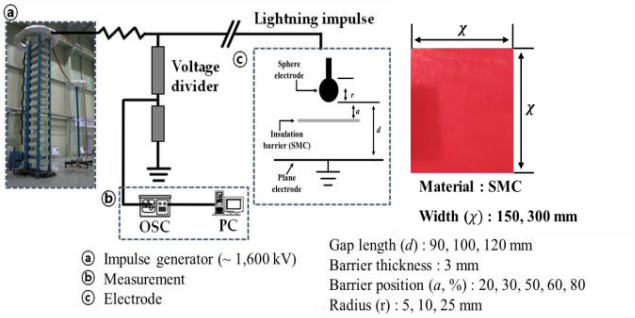

FIGURE 2. Experimental configuration and conditions of test electrodes.

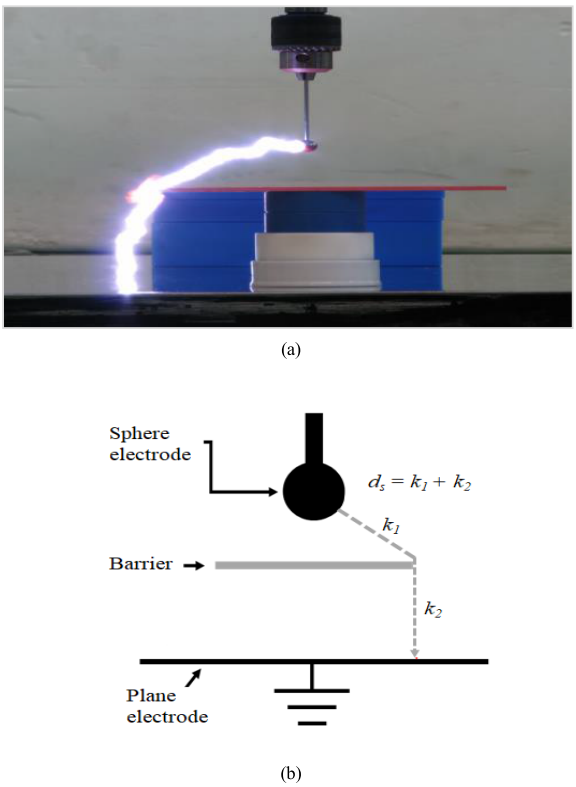

FIGURE 3. Discharge path and propagation length under sphere-to-barrier-to-plane: a) Bypass discharge, b) Depiction of streamer propagation length.

The lightning impulse generator delivers 1.2/50 us standard-waveform impulse voltages. The measuring system detects voltage waveforms using the voltage divider and stores them on PC. All breakdown experiments were conducted in an up and down method, and breakdown voltages were derived as the barrier width, the gap distance and the spherical radius all varied. Breakdown voltages were measured 15 times under each condition: calculated voltages are expressed as mean arithmetic values except for the maximum and minimum voltage.

Bypass discharge moved from the sphere to the barrier edge, and then to ground plane when sphere-to-barrier-to-plane electrodes were employed, as shown in Fig. 1(a).

TABLE 1. Breakdown voltages (V_{BD}) in sphere-to-barrier-to-plane (r: 5 mm).

Number	Position [%]	d_s	V_{BD} [kV]
d : 90 mm, barrier width : 150 mm			
1	20	138.7	125.1
2	50	124.2	112.2
3	80	115.4	105.2
d : 120 mm, barrier width : 150 mm			
4	20	165.1	143.5
5	50	155.7	135.4
6	80	140.5	125.5
d : 100 mm, barrier width : 150 mm			
7	20	159.9	128.2
8	30	152.7	120.1
9	50	141.5	115.2
10	60	137.2	112.4
11	80	130.5	109.5
d : 100 mm, barrier width : 300 mm			
12	20	233.9	156.6
13	30	225.4	153.6
14	50	210.2	146.1
15	60	203.5	143.8
16	80	191.6	136.8

TABLE 2. Breakdown voltages (V_{BD}) in sphere-to-barrier-to-plane (r: 10, 25 mm).

Number	Position [%]	d_s	V_{BD} [kV]
r : 10 mm, d : 90 mm, insulator width : 150 mm			
17	20	136.7	126.0
18	50	122.4	113.8
19	80	114.2	109.6
r : 10 mm, d : 120 mm, insulator width : 150 mm			
20	20	183.5	141.5
21	50	164.0	128.7
22	80	153.0	119.5
r : 25 mm, d : 100 mm, insulator width : 150 mm			
23	20	159.9	120.4
24	30	152.7	118.1
25	50	141.5	116.9
26	60	137.2	114.2
27	80	130.5	112.0

Neither puncture nor creepage discharges were considered during the breakdown experiments, because such discharges are uncommon in actual operation and the dielectric strength of the bypass discharge is higher. In a previous study, the discharge path length was used to identify how electrode shape varied by the barrier position, sphere radius and gap distance [29]. Because streamers are followed by discharges, the discharge path can be viewed as streamer propagation length (d_s) of equation (2), as plotted in Fig. 3(b). Table 1 and Table 2 list the experimental results.

$$d_s = k_1 + k_2, \tag{2}$$

where k_1 and k_2 are constants.

IV. ELECTRICAL CHARACTERISTICS OF SPHERE-TO-BARRIER-TO-PLANE

A. ELECTRO-GEOMETRIC EQUIVALENCY VARYING WITH RADII

Electro-geometric equivalency means that the breakdown voltages corresponding to the length of discharge (d_s) are nearly equal to those of bare electrodes with an air gap distance (d) identical to d_s [16]. The electro-geometric equivalencies of sphere-to-barrier-to-plane electrodes that differed in terms of spherical radii and barrier width were examined. The average electric field at a spherical radius of 5 mm differed from that at a spherical radius of 10 mm, leading to different electro-geometric equivalencies. All the breakdown voltages were also equivalent to an average electric field of a same field arrangement without barrier, regardless of the barrier width. The internal electric field of discharge channels were influenced more by spherical radii than by barrier width. Thus, propagation forces (Force = qE) depend on bare geometric shapes.

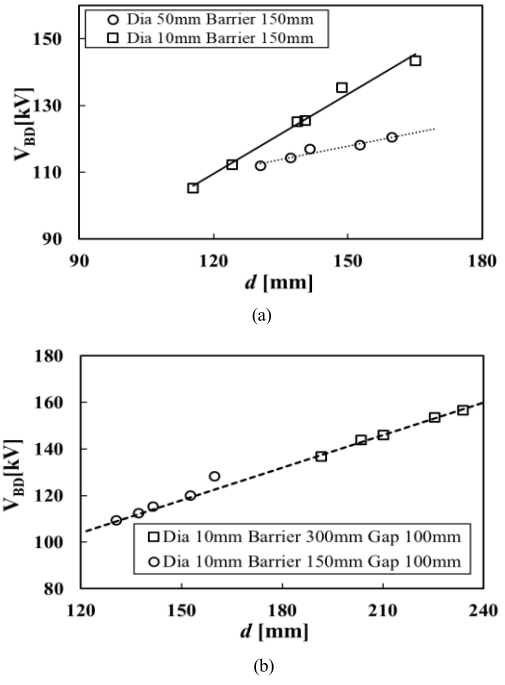

FIGURE 4. Electro-geometric equivalency by field arrangement: a) Spherical radii, b) Barrier width. (Solid line, dotted line: average electric field of each field arrangement without barrier, r: 5, 25 mm, d: 100 mm).

B. SEPARATION INTO TWO SUB-ELECTRIC FIELD DISTRIBUTIONS

The electric field distributions of air gaps were electrostatically examined along the shortest path from the sphere-to-barrier-to-plane. As shown in Fig. 5., electric fields exhibit different distribution depending on barriers. All electric fields featured two sub-electric fields, one of which was a non-uniform electric field between the sphere and the barrier, and the other was a quasi-uniform electric field between the

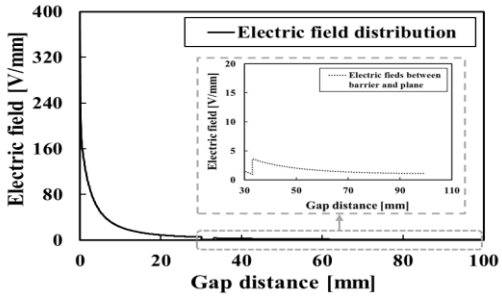

FIGURE 5. Electric field distribution along the shortest path. (*r*: 5 mm, barrier position [width]: 30 %, [150 mm], *d*: 100 mm).

barrier and the plane. Because electric fields between spheres and barriers change rapidly by gap distance, the non-uniform electric field described above was more important in terms of both discharge ignition and capacitive energy.

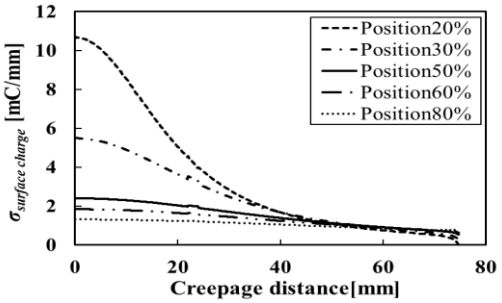

FIGURE 6. Charges by creepage distances from centers to edges by the barrier positions. (*r*: 5 mm, barrier width: 150 mm, *d*: 100 mm, 1 kV applied to sphere.).

C. SURFACE CHARGES AND EFFECT OF CHARGING ON DISCHARGE PATH

Surface charges are accumulated via the ionization (between molecules of air and electrons) and electric field acceleration. Surface charge distributions were investigated along the barrier creepage distance and varied by the barrier position, shown in Figure 6. Surface charges assume 'bell-shape', so as the barriers become closer to the sphere, the charge density rapidly rose in the center of the barrier and thus increasingly electrically shielded the sphere electrode potential. Surface charges move the ignition position from the center to a side, changing the discharge path and elongating the discharge length.

D. ELECTRICAL PROPERTIES FOR BYPASS DISCHARGE IN AIR GAPS

Streamers are followed by discharge channels. In the conceptual streamer involving positive ions (Figure 7(a)), internal fields of streamers are generated by such ions and have strengths in excess of 0.5 kV/mm at breakdown of 90 ∼ 95 % [14]. The internal field of discharge channels is also formed by positive ions but is lower than that of leader.

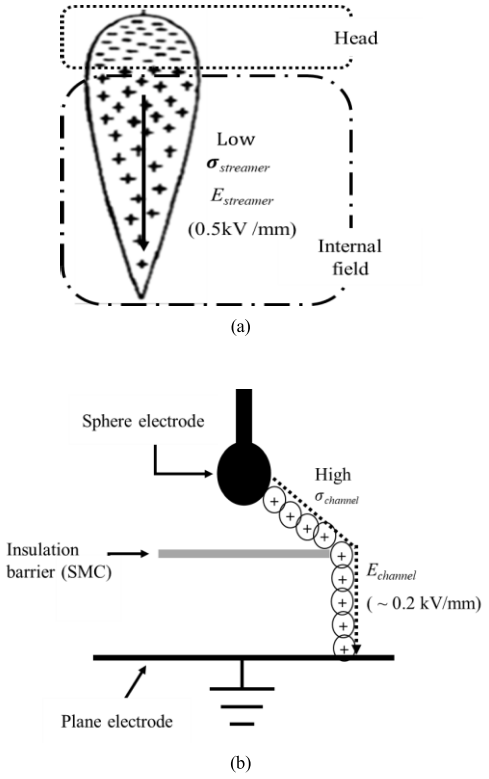

FIGURE 7. Electrical properties of streamers and discharge channels for bypass discharge: a) Conceptual streamer structure, b) Conceptual discharge channels. Dotted arrow is a discharge channel.

Therefore, the internal field of discharge channels may be lower than 0.2 kV/mm. Conductivity depends on the number of charged particles in channels. Discharge channels contain more charges than streamers, as confirmed by Gauss's law. Therefore, streamers have lower conductivities than discharge channels. Streamers may precede discharge propagation, so we examined stable streamer propagation at the critical electric field strength (0.5 kV/mm) to indirectly analyze discharge propagation in systems employing sphere-to-barrier-to-plane electrodes.

V. ELECTROSTATIC FIELD FEATURES FOR MACHINE LEARNING

The design of features is very important to predict breakdown voltages under the given test electrode. To show this point, usefulness of an optimization method (PCA) was explained [24], [25]. Various electrostatic field features are introduced in addition to the background electric field, to sufficiently reflect electrical characteristics over given test electrodes before and during discharge. Electrostatic field features are designed by the reference to electrical characteristics and the background electric fields affected by geometric shapes. Electrostatic field features can be divided into six groups: capacitive energy, electric field distribution, ionization characteristics, streamer propagation characteristics, surface charges and spatial inhomogeneities. According to previous studies, features involved background

electric field quantities corresponding to various electrode shapes such as rod-to-rod, sphere-to-plane and sphere-to-sphere air gaps [20] and SVM predicted voltages were well in agreement with experimental results. In our paper, both capacitive energy and electric field distribution were used as background electric field quantities under sphere-to-barrier and barrier-to-plane contexts, and were calculated along the shortest path. Furthermore, surface charging effect is considered varying with geometrical shapes, because charged values on the surface vary depending on the barrier position the gap distance and the radius. Consideration of ionization characteristics involved only the length required for charge generation. The streamer propagation characteristics reveal the electric potential drops required for stable propagation and the different electric forces needed to penetrate air gaps of varying geometric shapes. Moreover, such quantities can reflect environmental conditions and voltages waveforms by using E_{c0} term [15]. The streamer propagation characteristics are influenced by the internal electric field (E_{c0}) of streamer, which is known to be dependent on humidity, polarity and voltage waveform [13], [15]; since ambient air is considered in this paper, E_{c0} is 0.5 kV/mm; if dry air is used, E_{c0} can be 0.4 kV/mm; the value of E_{c0} may vary in the ranges of $+/-10 \sim 20$ % depending on humidity. Inhomogeneity reflects the spatial nonuniformities of both capacitive energies and discharge channel lengths.

TABLE 3. Electrostatic fields by feature groups.

Feature group	Notation
Capacitive energy	$C_s, C_{s\_SB}, C_{s\_ave}, C_{s\_BP}$
Electric field distributions	$E_{max}, E_{var}, E_{var\_SB}, E_{var\_BP}, E_{ave\_shortest}$
Ionization characteristics	L_E_{90}
Streamer propagation characteristics	$L_{st0.5}, V_{st0.5}, E_{ave\_SB}/E_{c0}, E_{ave\_BP}/E_{c0}$
Surface charges	$\sigma_{surface\_charges}$
Inhomogeneity	$C_{s\_SB}/C_s, C_{s\_BP}/C_{s\_SB}, L_{st0.5}/L_{dis}, L\_E_{90}/L_{dis\_SB}$

The electrostatic fields were defined as follows:

1. Total capacitive energy: C_s

$$C_s = \sum_{i=1}^{n} E_i^2 d_i, \tag{3}$$

where E_i and d_i are the electric field and the fine distance of the i-th element, and n is the sum of elements along the shortest path in air gaps.

2. Capacitive energy between sphere and barrier: C_{s_SB}

$$C_{s\_SB} = \sum E_i^2 d_i, \quad \text{where } i \text{ satisfy } \sum d_i \le d_{sp\_barrier}; \tag{4}$$

where $d_{sp\_barrier}$ is the distance between sphere and barrier along the shortest path in air gaps.

3. Average capacitive energy in air gaps: C_{s_ave}

$$C_{s\_ave} = C_s/n. \tag{5}$$

4. Capacitive energy between barrier and plane: C_{s_BP}

$$C_{s\_BP} = \sum E_i^2 d_i, \quad \text{where } i \text{ satisfy } \sum d_i \le d_{barrier\_plane}; \tag{6}$$

where $d_{barrier\_plane}$ is the distance between barrier and plane along the shortest path in air gaps.

5. Maximum electric field (along the shortest path): E_{max}

$$E_{max} = max E_i (i = 1, 2, 3, \ldots, n). \tag{7}$$

6. Average electric field between sphere and plane: $E_{ave\_shotest}$

$$E_{ave\_shortest} = \sum_{i=1}^{n} \frac{E_i}{n}. \tag{8}$$

7. Variance of electric fields in air gaps:

$$E_{var} = \frac{1}{n} \sum_{i=1}^{n} (E_i - E_{ave\_shortest})^2. \tag{9}$$

8. Variance of electric fields in air gpas between sphere and barrier: E_{var_SB}

$$E_{var\_SB} = \frac{1}{q_1} \sum_{i=1}^{q1} (E_i - E_{ave\_SB\_shortest})^2, \tag{10}$$

$$E_{ave\_SB\_shortest} = (\sum_{i=1}^{q1} E_i)/q_1, \tag{11}$$

where q_1 is the sum of a fine distance along the shortest path in air gaps between sphere and barrier.

9. Variance of electric fields in air gaps between barrier and plane: E_{var_BP}

$$E_{var\_BP} = \frac{1}{n - q_1} \sum_{i=1}^{n-q1} (E_i - E_{ave\_BP\_shortest})^2, \tag{12}$$

$$E_{ave\_BP\_shortest} = (\sum_{i=1}^{n-q1} E_i)/(n - q_1). \tag{13}$$

10. Penetration electric force in air gaps between sphere and barrier: E_{ave_SB} / E_{c0}

$$E_{ave\_SB}/E_{c0} = (\sum E_{dis\_i}/\sum i)/E_{c0}; \quad i \text{ satisfy } \sum l_i \le L_{dis\_SB}; \tag{14}$$

E_{dis_i} is the electric field of i-th element along the breakdown discharge path; l_i is the fine length along the discharge path; L_{dis_SB} is the length of discharge path from the sphere to the edge of barrier; E_{c0} is the critical electric field, 0.5 kV/mm [14].

11. Penetration electric force in air gaps between barrier and plane: E_{ave_BP}/E_{c0}

$$E_{ave\_BP}/E_{c0} = (\sum E_{dis\_i}/\sum i)/E_{c0}; \quad i \text{ satisfy } \sum l_i \le L_{dis\_BP}; \tag{15}$$

L_{dis_BP} is the length of discharge path from the edge of barrier to plane.

12. Length of electric potential drop in case that streamers stable proceed: $L_{st0.5}$

$$L_{st0.5} = \sum l_i, \quad \text{where } i \text{ satisfy } E_{dis\_i} \geq 0.5 \text{ kV/mm}. \tag{16}$$

13. Electric potential drop in case that streamers stable proceed: $V_{st0.5}$

$$V_{st0.5} = \sum E_{dis\_i} l_i, \quad \text{where } E_{dis\_i} \geq 0.5 \text{ kV/mm}. \tag{17}$$

14. Length of ionization: $L_{\_E90}$

$$L_{\_E90} = \sum d_i, \quad \text{where } i \text{ satisfy } E_i \geq E_{max} \times 0.9. \tag{18}$$

15. Surface charges: $\sigma_{surface\ charges}$

$$\sigma_{surface\_charges} = \epsilon_{ins} E_{n,ins,j}. \tag{19}$$

16. Relative capacitive energy: C_{s_SB}/C_s, C_{s_BP}/C_{s_SB}

17. Relative length: $L_{st0.5}/L_{dis}$, $L_{\_E90}/L_{dis\_SB}$ where L_{dis} is the total length of the discharge path from the sphere to the edge of barrier and from that edge to plane, and is equal to d_s; L_{dis_SB} is equal to k_1.

VI. MACHINE LEARNING ALGORITHMS AND PARAMETER TUNNING

A. SUPPORT VECTOR REGRESSION (SVR)

A SVR is a machine learning algorithm that solves nonlinear problems. The algorithm has one hidden layer. A ε-SVR determines the hyperplane on which losses (ε) are acceptable. The primary optimization problems are express by equation (20), where C and ε are hyperparameters [20], [21].

$$min\ \frac{1}{2} \| \omega \|^2 + C \sum\nolimits_{i=1}^{m} (\xi_i - \xi_i^*). \tag{20}$$

$$\text{s.t.} f(x_i) - y_i \leq \varepsilon + \xi_i. \tag{21}$$

$$y_i - f(x_i) \leq \varepsilon + \xi_i^*. \tag{22}$$

$$\xi_i, \xi_i^* \geq 0 \quad (i = 0, 1, 2, 3 \ldots n). \tag{23}$$

The decision function of ε-SVR is expressed by equation (24). The radial basis function (RBF) was used to map data from the original space to higher dimensions. γ is the Euclidean distance between two data points.

$$f(x) = \sum\nolimits_{i=1}^{m} (\alpha_i^* - \alpha_i) K(x, x_i) + b. \tag{24}$$

$$K(x, x_i) = \exp\left(-\gamma \| x_i - x_j \|^2\right). \tag{25}$$

B. BAYESIAN REGRESSION (BR)

Bayesian models are forms of artificial intelligence. Bayesian inference uses the prior probability and likelihood to estimate a posterior probability employing equation (26) [32].

$$p(x \mid E) = \int_0^x p(x \mid \theta)\, p(\theta \mid E)\, d\theta. \tag{26}$$

The posterior probability changes as new data are added. Posterior probabilities can serve as new prior probabilities, so automation of data inference is possible.

BR uses bayesian inference to regress an analysis between target (Y) and independent variables (X). The BR formula is expressed by equation (27) [32]. X contains n attributes including $x_1, x_2, \ldots$ and x_n; each is assumed to be independent; X, Y and ϵ are random variables; ϵ is a noise value. The hyperparameters are alpha and lambda.

$$Y = a + bX[n] + \epsilon[n]. \tag{27}$$

C. MULTILAYER PERCEPTRON (MLP) NEURAL NETWORK

Artificial neural network may be created using a multilayer perceptron (MLP) algorithm. Figure 8 shows conceptual MLP predicting breakdown voltages. A MLP features an input layer, an output layer, and a hidden layer. The input layer is a set of neurons that describe input features. Each neuron of the hidden layer transforms values from input layer via the weighted linear summation ($W_1X_1 + W_2X_2 + \cdots + W_mX_m$), followed by the activation function. The output layer transforms results of hidden layers into output values. In each neuron of the hidden layer, each parameter of (28) is trained. W_1 and W_2 are the weights of input and hidden layers. b_1 and b_2 are biases. Activation function (g) is 'identity' function. The solver uses "lbfgs". Since SVR has one hidden layer, the hidden layers in MLP were from 1 to 2. These algorithms are implemented with Scikit-learn library, which provides various modules associated with machine learning.

$$f(x) = W_2 g\left(W_1^T x + b_1\right) + b_2. \tag{28}$$

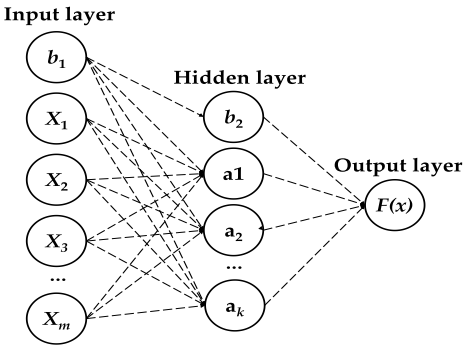

FIGURE 8. Conceptual multilayer perceptron.

D. NORMALIZATION AND PARAMETER TUNING

All the features were normalized to enhance predictive accuracy using equation (29).

$$X_i = \frac{x_i - x_{min}}{x_{max} - x_{min}}, \tag{29}$$

where X_i is a normalized value of an i-th input feature (x_i). x_{max} and x_{min} are the maximum and minimum values, respectively. K-fold cross-validation is employed with $K = 3$. The test dataset included samples that were randomly divided into three sub-datasets: two of these were used to train the SVR, BR and MLP models, and the other was used to validate the models. Gridsearch was employed to choose the hyperparameters and adjust the models.

E. CALCULATION OF PERMUTATION IMPORTANCES OF FEATURES

The permutation importances of features were investigated utilizing trained models that evaluated the test dataset; this ensured that feature overfitting was absent over the model. The importances are ordered by their R^2 scores, and only features that contributed more than 2 % to the predictions were shown.

VII. SIMULATION RESULT AND DISCUSSION

A. MODEL TRAINING AND TESTING

Datasets are crucial when seeking to enhance predictive accuracy. Three datasets are randomly grouped by d_s, as shown in Table 1 and Table 2. All samples were included in all datasets. The datasets that trained the SVR, BR and MLP models were randomly chosen: one of the three datasets was used for training and the others were used to test generalization afforded by the trained models and to analyze the predictive accuracies of breakdown voltages; these varied by the algorithm.

Two error indices were used when analyzing predicted breakdown voltages: the root mean square error (RMSE). The RMSE is defined by equation (30) and the MAPE is defined by equation (31).

$$\mathrm{RMSE} = \sqrt{\frac{1}{m}\sum_{i=1}^{m}(U_{bi} - U_{pi})^2}\ (\mathrm{kV}). \tag{30}$$

$$\mathrm{MAPE} = \frac{1}{m}\sum_{i=1}^{m}\left|\frac{U_{bi} - U_{pi}}{U_{bi}}\right|(\%), \tag{31}$$

where U_{bi} is the breakdown voltages and U_{pi} is the value predicted by SVR, BR and MLP. m is the number of total samples.

TABLE 4. Datasets and samples.

Dataset	Size	Sample number
1	9	5, 7, 11, 13, 14, 17, 19, 22, 27
2		2, 3, 4, 6, 9, 16, 21, 23, 26
3		1, 8, 10, 12, 15, 18, 20, 24, 25

TABLE 5. Error indices of predictions by three algorithms.

`	SVR		BR		MLP	
	MAPE	RMSE	MAPE	RMSE	MAPE	RMSE
1	0.878	1.571	0.841	1.525	1.820	3.009
2	0.483	0.798	0.497	0.935	1.048	1.9
3	0.999	1.563	1.120	2.253	1.019	1.725
Average	0.787	1.310	0.819	1.571	1.296	2.211
Variance	0.220	0.363	0.065	0.291	0.138	0.323

B. COMPARISON AMONG PREDICTED, CALCULATED AND EXPERIMENT BREAKDOWN VOLTAGES

Table 5 lists the error indices. Averages and variances were calculated for three all predictions. The average MAPE of the SVR and the BR were less than 0.9 %. The variance of MAPE of BR was the lowest. Although the BR MAPE variance was less than that of the SVR, the average BR MAPE was higher than that of the SVR. In terms of RMSE, SVR was more accurate than other algorithms. Therefore, VR optimally predicted the breakdown voltages of test electrodes.

SVR-predicted voltages were compared with both calculated voltages derived using the streamer propagation criterion and experimental results for an electrode of radius of 5 mm and a gap distance of 100 mm (Figure 9.). Voltages were calculated by the equation (32).

$$V = V_0 + E_{st} \cdot d_s, \tag{32}$$

where V_0 is equivalent to the required potential of head for breakdown; V_0 was 23.7 kV in the present study because the electrode shapes were very similar to those used in a prior work [33], [34]. In general, SVR-predicted voltages were in good agreement with experimental results at all barrier widths, but large differences were apparent between calculated and experimental results.

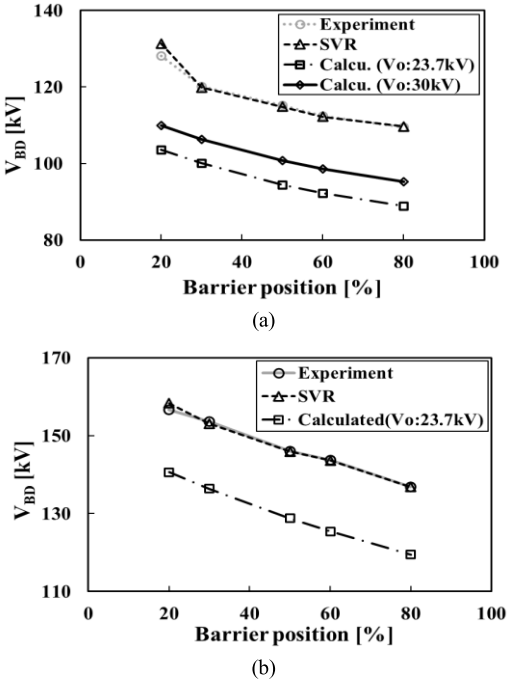

FIGURE 9. Comparison between SVR-predicted and calculated voltages by barrier width: a) 150 mm, b) 300 mm. (r: 5 mm, d: 100 mm).

The SVR-predicted voltages were compared with experimental results as the gap distance and the radius varied (Figure. 10 and 11). Predictions were in good agreement with experimental results as the gap distance under an electrode of radius of 5 mm and a barrier width of 150 mm varied. In case of the radius of 25 mm, a little deviation is observed at the barrier position of 30 and 50 %. Since the deviation is below 5 kV, the value is smaller than differences between breakdown voltages under experiment. Therefore, predictions were in good agreement with experimental results.

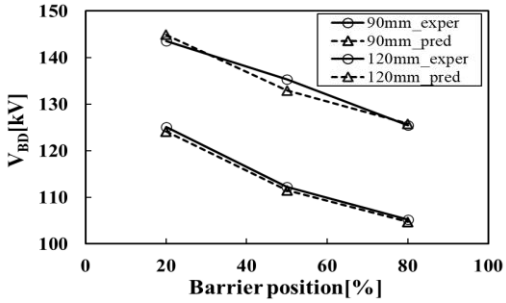

FIGURE 10. Comparison between SVR-predicted and experimental voltages by gap distance: experiment [exper], prediction [pred]. (*r*: 5 mm, χ: 150 mm).

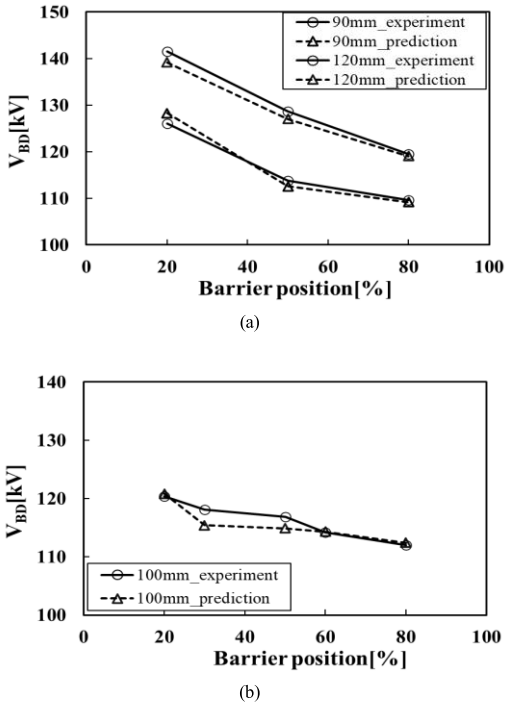

FIGURE 11. Comparison between SVR-predicted and experimental voltages by radii: a) 10 mm, b) 25 mm. (*d*: 100 mm, χ: 150 mm).

C. DISCUSSION

It is very difficult to predict the breakdown voltages of the sphere-to-barrier-to-plane electrodes, given the nonlinear relationships between the suggested features and the electron generation affecting both discharge ignition and discharge propagation. Each suggested feature not only affects each other, but also combines complexly to contribute to nonlinear collision ionization which generates electrons. Machine learning identifies the influence of each feature affecting the electron generation to predict breakdown voltages. The predictions of machine learning algorithms were in good agreement with experimental results. Although SVR has one hidden layer and is simple, it was more accurate and efficient than the MLP. The most significant features affecting breakdown voltages are the length of the electric potential drop

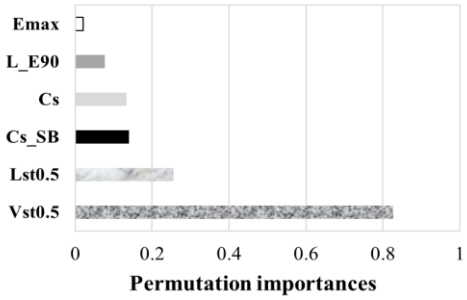

FIGURE 12. Permutation importances of features in SVR-trained model operating on a test dataset. (importance order: 1 to 6).

($L_{st0.5}$) and the electric potential drop ($V_{st0.5}$) per se, which influence stable discharge penetration into air, as shown in Figure 12. Our findings demonstrate that machine learning can evaluate breakdown voltages well, and can also reflect the electrical properties required for streamer propagation. Therefore, machine learning can be used to analyze breakdown accidents in industrial fields.

The utilization factor is approximately 0.0271 in a sphere-to-barrier-to-plane with a spherical radius of 5 mm and a gap distance of 100 mm; the electric field distribution is thus strongly inhomogeneous. Accordingly, streamer propagation was used to predict the breakdown voltages. To this end, an equivalent potential (V_0) is experimentally required when the electrode shapes vary. V_0 can range from 20 to 30 kV [34], and large deviation were observed even when V_0 was 30 kV (Figure. 9(a)). However, machine learning affords higher predictive accuracy than the theoretical approach and can consider electric field distribution of geometrical electrode shapes. Unlike traditional theoretical approaches, the proposed method does not need to confirm whether the electric distributions corresponding to geometrical shapes are applicable. The method can predict breakdown voltages through the computational analysis without experimental data required to consider electron generation. Nevertheless, if the shape of barrier surface is not flat and becomes complex, it is necessary to add the physical characteristics as an input parameter. Moreover, area effect may be considered in case that the radius is larger than a certain value. When the radius of the active (high voltage) electrode is larger than a certain value, the area effect occurs, and breakdown voltages may be influenced by the increase in the effective area of the electric field with larger than 90% of the maximum electric field. In case of compressed gases such as dry air and SF_6, surface roughness may be included, which is associated with the discharge ignition [35].

VIII. CONCLUSION

In this paper, positive lightning impulse breakdown voltages in the sphere-to-barrier-to-plane scenario were predicted by machine learning algorithms. The breakdown voltages are rarely analyzed using such algorithms. Unlike previous studies, features of the background electric fields and the

penetration characteristics of discharge channels in air gaps were used, when evaluating the physical electrical characteristics, yielding enhanced predictive accuracy for the electrodes described above. The predictive accuracies of the SVR, BR, and MLP were assessed, and predicted voltages were compared with both the experimental results and voltages calculated using the streamer propagation characteristics.

1) Electro-geometric equivalencies and stable streamer internal fields were used to describe the discharge channels. Surface charges and sub-electric field distribution between spheres and barriers, or between barriers and planes, were employed to describe the background electric fields of each electrode shape.

2) SVR-predicted voltages were more accurate than those of BR and MLP. The SVR thus optimally evaluated the breakdown voltages of the studied electrodes.

3) At a spherical radius of 5 mm and a gap distance of 100 mm (associated with a strongly inhomogeneous field), SVR-predicted voltages were in line with experimental results, but large differences were apparent between the experimental and the calculated voltages estimated using a stable internal field of 0.5 kV/mm and an equivalent potential (V_0) of 23.7 kV.

4) Overall, SVR-predicted voltages were in good agreement with experimental results regardless of differences in geometric parameters such as spherical radius, gap distance, and barrier width.

5) Discharge channel characteristics best played a role in predicting the breakdown voltages. This is because such properties indirectly represent the equivalent gap distances that affect the breakdown voltage in the sphere-to-barrier-to-plane scenario.

The features of the proposed method effectively aided machine learning, enabling the prediction of breakdown voltages without the need to consider field distribution when the streamer propagation is in play. The proposed method physically explains the important electrical properties affecting discharge under such conditions, so it will be of great benefit to discharge analyses associated with power equipment operation. Further studies will explore different applied voltage shapes and more complex creepage structure. Also, comparison on performance of different machine learning algorithms on such problems, as well as main factors affecting prediction accuracy will be conducted over various geometrical shapes.

REFERENCES

[1] *High-Voltage Switchgear and Controlgear—Part 100: Alternating-Current Circuit Breakers*, Standard IEC 2271-100, 2021.
[2] M. Klas, Š. Matejcík, B. Radjenovic, and M. Radmilovic-Radjenovic, "Experimental and theoretical studies of the breakdown voltage characteristics at micrometre separations in air," *EPL Europhysics Lett.*, vol. 95, no. 3, Aug. 2011, Art. no. 35002.
[3] A. P. Jovanovic, M. N. Stankov, V. L. Markovic, and S. N. Stamenkovic, "The validity of the one-dimensional fluid model of electrical breakdown in synthetic air at low pressure," *EPL Europhysics Lett.*, vol. 104, no. 6, Dec. 2013, Art. no. 65001.
[4] M. Seeger, L. Niemeyer, and M. Bujotzek, "Partial discharges and breakdown at protrusions in uniform background fields in SF6," *J. Phys. D, Appl. Phys.*, vol. 41, no. 18, Sep. 2008, Art. no. 185204.
[5] M. Seeger, L. Niemeyer, and M. Bujotzek, "Leader propagation in uniform background fields in SF6," *J. Phys. D, Appl. Phys.*, vol. 42, no. 18, Sep. 2009, Art. no. 185205.
[6] M. Seeger and M. Clemen, "Partial discharges and breakdown in SF6 in the pressure range 25–150 kPa in non-uniform background fields," *J. Phys. D, Appl. Phys.*, vol. 47, no. 2, Jan. 2014, Art. no. 025202.
[7] A. Pedersen, "Criteria for spark breakdown in sulfur hexafluoride," *IEEE Trans. Power App. Syst.*, vols. PAS-89, no. 8, pp. 2043–2048, Nov. 1970.
[8] M. Tefferi, F. Pyle, A. Laso, A. Dauksas, K. Darko, N. Uzelac, A. Scott, and W. Xu, "Streamer criterion for designing gas-insulated medium voltage switchgear," in *Proc. IEEE Conf. Electr. Insul. Dielectric Phenomena (CEIDP)*, Denver, CO, USA, Oct. 2022, pp. 451–454.
[9] W. S. Zaengl and K. Petcharaks, "Application of streamer breakdown criterion for inhomogeneous fields in dry air and SF6," in *Gaseous Dielectrics VII*. Cham, Switzerland: Springer, 1994, pp. 153–159.
[10] K. Petcharaks, "A contribution to the streamer breakdown criterion," in *Proc. 11th Int. Symp. High-Voltage Eng.*, 1999, pp. v3–19.
[11] A. Pedersen, "On the electrical breakdown of gaseous dielectrics—An engineering approach," *IEEE Trans. Electr. Insul.*, vol. 24, no. 5, pp. 721–739, 1989.
[12] N. Malik, "Streamer breakdown criterion for compressed gases," *IEEE Trans. Electr. Insul.*, vols. EI-16, no. 5, pp. 463–467, Oct. 1981.
[13] A. Pedersen and A. Blaszczyk, "An engineering approach to computational prediction of breakdown in air with surface charging effects," *IEEE Trans. Dielectr. Electr. Insul.*, vol. 24, no. 5, pp. 2775–2783, Oct. 2017.
[14] N. L. Allen and P. N. Mikropoulos, "Dynamics of streamer propagation in air," *J. Phys. D, Appl. Phys.*, vol. 32, no. 8, pp. 913–919, Apr. 1999.
[15] A. Pedersen, T. Christen, A. Blaszczyk, and H. Boehme, "Streamer inception and propagation models for designing air insulated power devices," in *Proc. IEEE Conf. Electr. Insul. Dielectric Phenomena*, Oct. 2009, pp. 604–607.
[16] A. Beroual and A. Boubakeur, "Influence of barriers on the lightning and switching impulse strength of mean air gaps in point/plane arrangements," *IEEE Trans. Electr. Insul.*, vol. 26, no. 6, pp. 1130–1139, Jul. 1991.
[17] M. A. A. Wahab, "Artificial neural network-based prediction technique for transformer oil breakdown voltage," *Electr. Power Syst. Res.*, vol. 71, no. 1, pp. 73–84, Sep. 2004.
[18] S. S. M. Ghoneim, S. S. Dessouky, A. A. Elfaraskoury, and A. B. A. Sharaf, "Prediction of insulating transformer oils breakdown voltage considering barrier effect based on artificial neural networks," *Electr. Eng.*, vol. 100, no. 4, pp. 2231–2242, Dec. 2018.
[19] J. S. Foo and P. S. Ghost, "Artificial neural network modelling of partial discharge parameters for transformer oil diagnosis," in *Proc. Annu. Report Conf. Elect. Insul. Dielectric Phenomena*, 2002, pp. 470–473.
[20] Z. Qiu, J. Ruan, D. Huang, Z. Pu, and S. Shu, "A prediction method for breakdown voltage of typical air gaps based on electric field features and support vector machine," *IEEE Trans. Dielectr. Electr. Insul.*, vol. 22, no. 4, pp. 2125–2135, Aug. 2015.
[21] Z. Qiu, J. Ruan, W. Xu, and C. Huang, "Breakdown voltage prediction of rod-plane gap in rain condition based on support vector machine," in *Proc. IEEE Int. Conf. High Voltage Eng. Appl. (ICHVE)*, Sep. 2016, pp. 1–4.
[22] Y. Qin, X. Li, B. Ren, Q. Yan, and K. He, "Prediction of switching impulse breakdown voltage of the air gap between tubular buses in substation," in *Proc. 4th Int. Conf. Smart Power Internet Energy Syst. (SPIES)*, Dec. 2022, pp. 9–13.
[23] Z. Qiu, L. Zhang, Y. Liu, J. Liu, H. Hou, and X. Zhu, "Electrostatic field feature selection technique for breakdown voltage prediction of sphere gaps using support vector regression," *IEEE Trans. Magn.*, vol. 57, no. 6, pp. 1–4, Jun. 2021.
[24] Z. Qiu, J. Ruan, D. Huang, M. Wei, L. Tang, and S. Shu, "Corona onset and breakdown voltage prediction of rod-plane air gaps based on SVM algorithm," in *Proc. IEEE Conf. Electr. Insul. Dielectric Phenomena (CEIDP)*, Oct. 2015, pp. 217–220.
[25] Z. Qiu, J. Ruan, D. Huang, M. Wei, L. Tang, C. Huang, W. Xu, and S. Shu, "Hybrid prediction of power frequency breakdown voltage of short air gaps," *IEEE Trans. Dielectr. Electr. Insul.*, vol. 23, no. 2, pp. 795–805, Jul. 2016.

[26] S. Akram, P. Wang, X. Zhu, J. Huang, F. Liu, Z. Fang, and H. Ahmed, "Prediction of partial discharge inception voltage for electric vehicle motor insulation using deep learning," *IEEE Trans. Instrum. Meas.*, vol. 72, pp. 1–10, 2023.

[27] C. Peng, X. Dong, J. Ruan, Y. Zhao, B. Luo, T. Wang, and S. Cheng, "Deep learning-based breakdown voltage prediction for ball-to-ball discharge with an air gaps less than 1.5 m," in *Proc. 10th Frontier Academic Forum Elect. Eng.*, 2023, pp. 1293–1301.

[28] I.-H. Kim, J.-H. Bong, J. Park, and S. Park, "Prediction of driver's intention of lane change by augmenting sensor information using machine learning techniques," *Sensors*, vol. 17, no. 6, p. 1350, Jun. 2017.

[29] B. Y. Seok, "Electrical breakdown characteristics in non-uniform electrode system with bakelite barrier under the lightning impulse voltage," *Electr. Eng.*, vol. 102, pp. 2263–2368, Jun. 2020.

[30] H. K. Meyer, A. Blaszczyk, M. Schueller, F. Mauseth, and A. Pedersen, "Surface charging of dielectric barriers in short rod-plane air gaps-experiments and simulations," in *Proc. IEEE Int. Conf. High Voltage Eng. Appl. (ICHVE)*, Athens, Greece, Sep. 2018, pp. 1–4.

[31] H. K. Meyer, F. Mauseth, R. Marskar, A. Pedersen, and A. Blaszczyk, "Streamer and surface charge dynamics in non-uniform air gaps with a dielectric barrier," *IEEE Trans. Dielectr. Electr. Insul.*, vol. 26, no. 4, pp. 1163–1171, Aug. 2019.

[32] K. J. Park and T. H. Kim, "Forecasting demand of 5G Internet of Things based on Bayesian regression model," *J. Inf. Technol. Appl. Manage.*, vol. 26, pp. 61–73, Jul. 2019.

[33] F. Mauseth, J. S. Jørstad, and A. Pedersen, "Streamer inception and propagation for air insulated rod-plane gaps with barriers," in *Proc. Annu. Rep. Conf. Electr. Insul. Dielectric Phenomena*, Oct. 2012, pp. 732–739.

[34] E. Nasser, "Der raumliche entladungsaufbau im ungleichformigen feld bei positiver spitze in atmospharischer luft," *Archiv Fur Elektrotechnik*, vol. 44, no. 3, pp. 157–167, Mar. 1959.

[35] S. Berger, "Onset or breakdown voltage reduction by electrode surface roughness in air and SF6," *IEEE Trans. Power App. Syst.*, vols. PAS-95, no. 4, pp. 1073–1079, Jul. 1976.

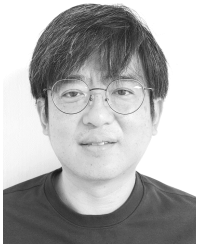

JIN-TAE KIM received the B.S. degree in electrical engineering from Kyungpook National University, Daegu, in 2006, and the M.S. degree in electrical engineering from Seoul National University, Seoul, South Korea, in 2008. He is currently pursuing the Ph.D. degree with the Graduate School of Energy Convergence, the Gwangju Institute of Science and Technology (GIST). He had been a Senior Researcher with Hyundai Heavy Industries Company Ltd., from 2010 to 2016. Since 2016, he has been a Senior Researcher with Korea Electric Power Research Institute (KEPRI). His current research interests include high voltage phenomena, insulation design of high voltage electric power apparatus, energy storage systems, power forecast of wind turbine and artificial intelligence.

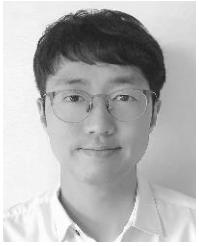

YUN-SU KIM (Senior Member, IEEE) received the B.S. and Ph.D. degrees in electrical engineering from Seoul National University, Seoul, South Korea, in 2010 and 2016, respectively. He was a Senior Researcher with Korea Electrotechnology Research Institute (KERI), from 2015 to 2017. He joined Gwangju Institute of Science and Technology (GIST), as a Faculty Member, in 2018, where he is currently an Associate Professor with the Graduate School of Energy Convergence. His research interests include distribution networks, distributed energy resources, microgrids, and artificial intelligence. He was the Director of Korean Society for New and Renewable Energy and Korean Institute of Electrical Engineers.